2020년 8월

박사학위 논문

Photoluminescent Rugate and Bragg Porous Silicon Interferometers for Enhanced Detection of Organic Vapors

조 선 대 학 교 대 학 원

화 학 과

주 자 성

Photoluminescent Rugate and Bragg Porous Silicon Interferometers for Enhanced Detection of Organic Vapors

유기물 증기의 향상된 감지를 위한 광발광성 브래그 및 루게이트 다공질 실리콘 간섭계

2020년 8월 28일

조 선 대 학 교 대 학 원

화 학 과

주 자 성

Photoluminescent Rugate and Bragg Porous Silicon Interferometers for Enhanced Detection of Organic Vapors

지도교수 손 홍 래

이 논문을 이학박사학위신청 논문으로 제출함.

2020년 05월

조 선 대 학 교 대 학 원

화 학 과

주 자 성

주자성의 박사학위논문을 인준함

위원장 조선대학교 교수 김 호 중 (인)

위 원 조선대학교 교수 고 문 주 (인)

위 원 조선대학교 교수 손 홍 래 (인)

위 원 조선대학교 교수 이 종 대 (인)

위 원 세한대학교 교수 고 영 춘 (인)

2020년 7월

조 선 대 학 교 대 학 원

TABLE OF CONTENTS

LIST OF SYMBOLS AND ABBREVIATIONS

PSi	porous silicon
DBR	Distributed Bragg Reflector
FE-SEM	Field Emission-Scanning Electron Microscope
PL	photoluminescence
HF	Hydrofluoric Acid
FWHM	full width at half maximum
UV	ultraviolet
QD	quantum dots
μm	micrometer
mA	milliampere
cm	centimeter
min	minute
sec	second
LED	light-emitting diode
nm	nanometer
Ω	Ohm
L	low
H	high

LIST OF FIGURES AND TABLES

PART 1

A Novel Chemical Gas Vapor Sensor Based on Photoluminescence Enhancement of Rugate Porous Silicon filters

PART 2

Enhanced Detection of Organic Vapors Based on Photoluminescent Distributed Bragg-Reflective Porous Silicon Interferometer

초 록

향상된 유기물 증기 감지를 위한 광발광성 브래그 및 루게이트 다공질 실리콘 간섭계

박사과정 : 주 자 성
지도교수 : 손 홍 래
조선대학교 화학과

분산 브래그 반사경(DBR)과 루게이트 PSi를 포함한 다층 다공성 실리콘(PSi) 광 발광체가 조명 하에서 실리콘 웨이퍼에 여러 차례 서로 다른 특정 전류 밀도를 주는 전기화학적 에칭을 통해서 발견되었다. 제조된 DBR 및 루게이트 PSi는 단층 PSi와 비교하여 특이한 반사 및 광 발광성 특성을 모두 갖는다. DBR, 루게이트 PSi은 반사 및 광 발광에서 우수한 광학적 특성을 나타내는데 SEM 기기를 이용하여 광학적 특성의 메카니즘을 분석하였다. DBR 및 루게이트 PSi의 광학적 특성을 연구하여 유기 증기를 감지하는 데 이용하였다.

DBR, PSi 샘플은 조명 하에서 80회 반복되는 주기적 구형파 전류를 이용하는 전기화학 에칭을 이용하여 제조하였다. 단면 SEM 이미지를 이용하여 DBR, PSi은 다공성 실리콘 층의 다른 형태의 구조를 가지고 있음을 발견하였다. DBR, PSi의 반사 적색 이동 및 광 소광 둘 모두를 유기 증기의 노출 하에서 측정하였다. 그 결과 톨루엔, 헥세인 및 클로로폼에 노출되었을 때 반사 적

색 이동 및 PL 소광 크기에서 상당한 차이를 나타냈다. DBR의 광 소광이 단층 PSi의 경우보다 컸다. 반사 적색 이동은 증기압에 의해 영향을 받았으며, PL 소광은 따라서 DBR PSi는 PL 소광과 반사적 색 이동에 기반을 둔 화학 증기 센서로 이용될 수 있다.

루게이트 PSi 샘플은 10 사이클의 주기적인 정현파 전류를 사용하여 조명 하에서 전기화학적 에칭에 의해 제조하였다. 루게이트 PSi의 단면 이미지는 정현파 다공질 층에 따라 점진적이고 규칙적으로 변화하는 특수 스트라이프 구조를 나타낸다. 이러한 다공성 층은 정현파의 식각 전류와 일치한다. 유기 증기의 노출하에서 루게이트 PSi 필터의 반사 적색 이동 및 PL 소광을 측정하였다. 그 결과 톨루엔, 헥산 및 클로로폼 감지를 위한 반사 적색 편이 및 PL 소광 크기가 상당한 차이를 나타냈다. 루게이트 PSi 샘플의 PL 소광 백분율이 단층 PSi의 것 보다 컸다. 이 결과는 루게이트 PSi 필터의 반칙폭이 작은 PL 피크가 단층 PSi의 반칙폭이 넓은 PL보다 더 민감하다는 것을 나타냈다. 반사 적색 이동 및 PL 소광은 유기 종의 증기압 및 쌍극자 모멘트에 의해 영향을 받았다.

Part 1

A Novel Chemical Gas Vapor Sensor Based on Photoluminescence Enhancement of Rugate Porous Silicon filters

1.1. Introduction

Since the discovery of its photo- and electro-luminescence characteristics [1,2], the fabrication of porous silicon (PSi) has been intensively researched for various applications such as chemical sensors[3], biological sensors [4], drug delivery systems [5], and medical diagnostics [6]. PSi is an ideal candidate material used in gas and liquid-sensing applications due to its sponge structure with a high surface-to-volume ratio, various orientation of pores, and the size of pore diameters that can be altered by changing the production conditions [7,8]. The sensing techniques that have been mainly investigated to achieve signal transduction on basis of capacitance [9], resistivity [10], reflection [11], photo-luminescence (PL) [12,13], etc. However, optical measurements for detection applications have demonstrated high sensitivity and potentially greater capability for the identification of specific adsorbates.

To the best of our knowledge, PL emission is most likely due to the quantum confinement effects within silicon quantum dots. Enhancement of PL is critical for improving the detection quality. It was reported in the literature that increasing radiative recombination via direct band-gap transitions and reducing the phonon-assisted indirect band-gap transitions can significantly enhance the photoluminescence [14]. Previous studies led by our group have demonstrated the successful fabrication of the DBR multilayer PSi devices exhibiting narrow PL peaks arising from Bragg resonance during the visible wavelength range [15]. DBR PSi devices are produced by alternating the square wave current between low and high values, leading to alternating PSi multilayers with high and low refractive indices, respectively. Nevertheless, if the current is changed gradually, PSi with a smooth variation in the refractive indices along with etching direction can be achieved, obtaining the so-called rugate PSi. In this work, luminescent rugate PSi with narrow and strong PL was prepared using a highly doped n-type silicon wafer under illumination. We designed the reflection peak that is

reflected exclusively in the range of the rugate PL wavelength position and constructively propagates with the overlapping emission domain of the optical Si quantum dots, thus amplifying the PL intensity. As far as we are aware, the present work is the first demonstration of the use of this approach for PL enhancement.

The PL efficiency of PSi relies on the interior diverse structures and the versatile surface properties [16]. Organic vapors have been detected by PL quenching due to the differences in the physicochemical properties between the organic molecules [17]. Here, we report a method for the preparation of photoluminescent rugate PSi exhibiting both well reflection and PL based on highly doped n-type silicon wafers. The PL enhanced by constructive propagation with reflection from porous silicon was used for the detection of the vapor pressure of organic solvents.

1.2. Experiments

1.2.1. Materials

n++-type (0.001 ~ 0.003 Ω•cm) and n-type (1 ~ 10 Ω•cm) single-side polished <100> oriented silicon wafer (Prime grade, Siltronix Inc., Archamps, France),HF (48 - 51%, ACS Reagent, J.T. Baker, PA, USA), ethanol (99.8%, Merck, Darmstadt, Germany), toluene (99.5%, ACS reagent, Aldrich Chemicals, Sigma-Aldrich, Steinheim, Germany), hexane (95%, ACS reagent, Aldrich Chemicals, Sigma-Aldrich, Steinheim, Germany), and chloroform (>99.5%, ACS reagent, Aldrich Chemicals, Sigma-Aldrich, Steinheim, Germany) were used as received.

1.2.2. Preparation of Rugate PSi

Rugate PSi filters samples were prepared by an electrochemical anodization of an n^{++}-type(0.001-0.003Ω•cm). Anodization was performed by a Teflon cell and a Pt ring as the counter electrode at room temperature in a mixed solution with 50% volumetric fraction of aqueous HF and absolute ethanol. The applied current density was controlled using a Keithley 2420 high-precision constant current source (Keithley Instruments Inc., USA). The current waveform used in this work is an individual sine component that is represented as:

$$y = A\sin(kt) + B \qquad (1)$$

where y represents a temporal sine wave with amplitude A, frequency k, time t, and an applied current density B. The values for A, k, t, and B were set to 60.55, 1.02, 1000, and 110, respectively.

Gradually varied etching controlled by sinusoidal current was performed under the illumination by a tungsten filament bulb(300-W) during the whole etching. For comparison, a monolayer PSi with a broad PL peak was fabricated by n-type silicon

wafer(1 ~ 10Ω•cm) by ethanol several times and dried with argon atmosphere prior to use.

1.2.3. Instruments and Data Acquisitions

PL steady-state spectra were obtained using an Ocean Optics S2000 spectrometer fitted with a fiber optic probe. The excitation source was a LED (λmax = 460 nm) focused on the sample surface (at an angle of 45^{o} to the normal of the surface) using a separate fiber. Light was collected at the direction of an angle of 90^{o} to the normal of the surface using an optical fiber. The spectra of wavelength for 400 ~ 900 nm were measured and recorded by a CCD-detector. Percentage of quenching values are calculated by $(I_0-I)/I_0$, where I_0 is the initial PL intensity of the rugate PSi samples in the wavelength of 400 ~ 900 nm, I is the integrated PL intensity of the rugate PSi in the presence of quencher(analyte). The interferometric reflectance spectra of the rugate PSi samples were measured under a tungsten filament lamp, focused on the center of the rugate PSi surface and recorded by an Ocean Optics S2000 spectrometer. The reflectance spectra were recorded by a CCD detector with wavelength of 400 ~ 1200 nm.The direction of illuminations as well as the detection of the reflected light were performed along an angle of 90^{o} to the surface normal. At least three times of measurements were performed for each analyte detection. The morphologies of rugate and monolayer PSi samples were characterized using cold field emission scanning electron microscopy (FE-SEM, S-4800, Hitachi, Ltd., Chiyoda, Tokyo, Japan).

1.2.4. Characterization

Morphologies of PSi samples were obtained by a cold field emission scanning electron microscopy (FE-SEM, S-4800, Hitachi).

1.2.5. Detection of Organic Vapor

The effectiveness of the amplified PL in regards to detection performance by rugate PSi was examined by sensing organic solvents. The results of organic vapor detection performance by rugate PSi were compared with monolayer PSi. The rugate PSi were placed in an exposure chamber fitted with an optical window, and toluene, hexane, and chloroform were used to investigate the adsorption behavior. Argon gas was used as the carrier gas for the volatile organic compound vapors, and the analyte concentration in carrier gas was adjusted by the flow meters. The influence of different organic species vapors namely, toluene, hexane, and chloroform on the PL spectra of rugate PSi were studied. All sensing measurements were carried out at room temperature. Figure 1.1 showed a schematic diagram for the gas sensing system. We measured the PL of rugate PSi in the presence of different organic species with various vapor concentrations at the same carrier gas flow.

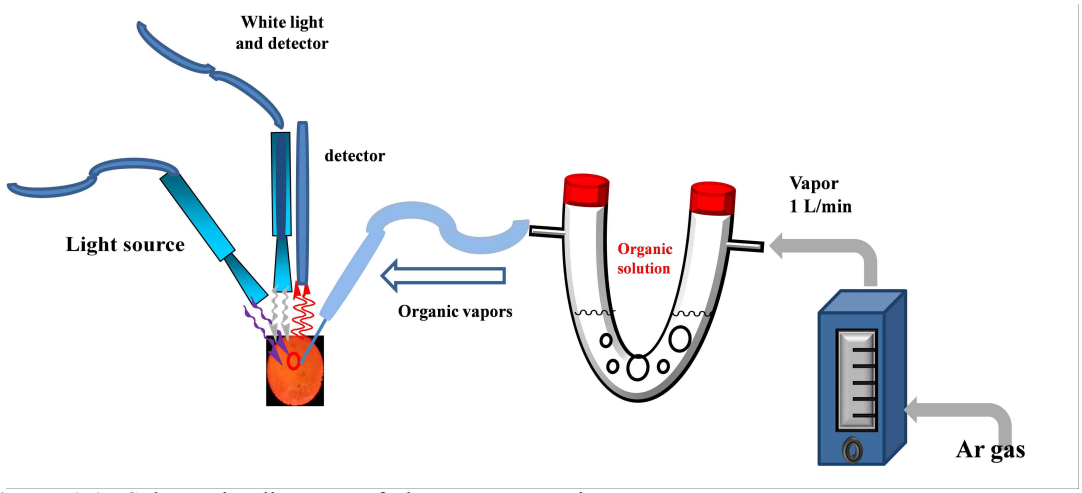

Figure 1.1. Schematic diagram of the gas measuring system

1.3. Results and Discussion

Rugate PSi exhibiting narrow peaks for both reflectance and PL was successfully fabricated by applying gradually varied current waveform under illumination with a tungsten filament bulb with the power of 300 W during etching. Photographs of rugate PSi under visible light and UV light are shown in Figure 1.2. Plotted together, the reflection and PL spectra (Figure 1.3) show that the position of the PL peak from rugate PSi coincides with the reflection peak of rugate PSi at 663 nm with a full width at half maximum (FWHM) of 22 nm. Thus, the optical peak was enhanced because the photoluminescence propagated constructively with reflectance. In contrast, the optical spectra of monolayer PSi displayed a broad PL spectrum with 154 nm of FWHM.

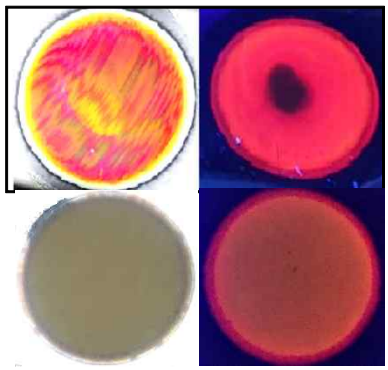

Figure 1.2. Photographs of rugate PSi (upper) and monolayer PSi(below) samples under visible light (left) and ultraviolet light (right). Dark area of the red luminescent region in rugate PSi represents the quenching of PL with a drop of hexane.

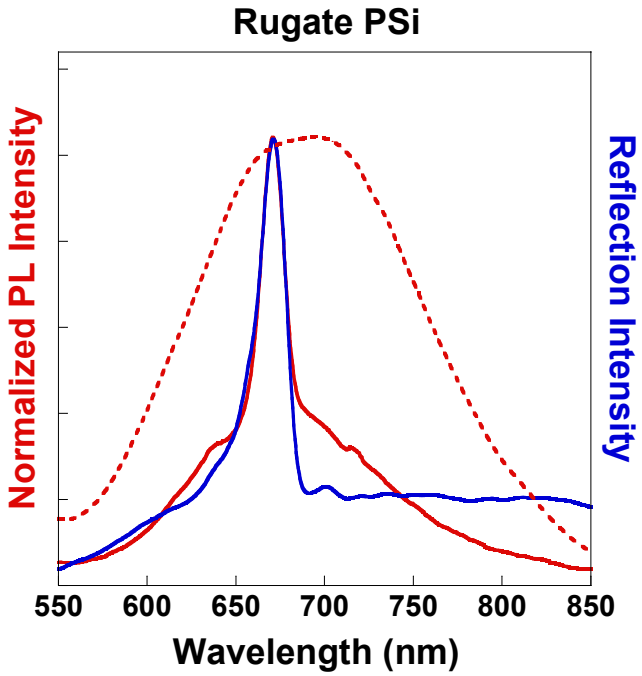

Figure 1.3. PL (red line) and reflectance (blue line) spectra of the prepared rugate PSi and PL (red dot) spectrum of the monolayer PSi.

The rugate PSi having gradually modulated refractive indices with sinusoidal porosity exhibits a narrow and high reflection band. However, monolayer PSi having constant refractive index with cylindrical pore exhibits a lack of reflection features. For photoluminescence, the PL of monolayer and rugate PSi is triggered by the quantum confinement of silicon quantum dots (QDs) on the surface of PSi. Figure 1.4A and 1.4B displays schematic illustrations for rugate and monolayer PSi, respectively. Figure 1.4C shows that the emission spectrum of Si QDs in rugate PSi was substantially narrowed and amplified after passing through the special and repeated multilayers of rugate structure. However, the emission spectrum of monolayer PSi showed a broad PL band due to the lack of rugate filter.

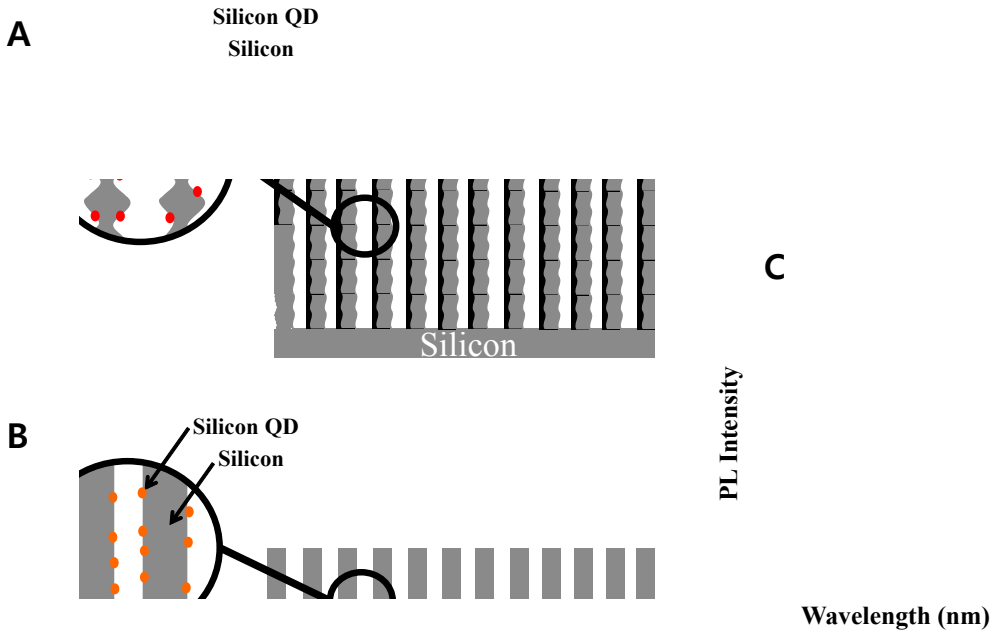

Figure 1.4. Schematic illustration of (A) rugate PSi and (B) monolayer PSi. PL spectra for (C) rugate PSi (solid line) and monolayer PSi (dotted line).

Figure 1.5 shows the SEM images of the surface and cross-sectional views of the rugate and monolayer PSi. Figure 1.5A showed that the rugate PSi prepared with 10 cycles exhibited a flat surface with the pore sizes in the 10–20 nm range. The total thickness of the rugate and monolayer PSi were approximately 88.5 and 82.5 μm, respectively. Rugate PSi shown in Figure 1.5B is composed of a regularly changing special stripe structure that is gradually varied with the sinusoidal porous layers. This gradually varied porous layer is consistent with the alternating sinusoidal etching current. By contrast, a cylindrical pore structure for the monolayer PSi that was

fabricated using a constant etching current was generated (Figure1.5C and D).

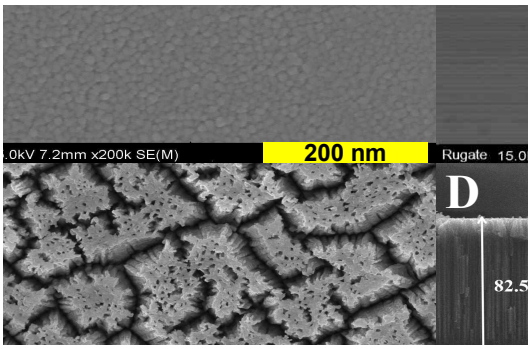

Figure 1.5. Top surface and cross-section SEM images of rugate PSi (A1-A3) and monolayer Si (B1,B2).

As shown in Figure 1.6, organic vapors were adsorbed on the pore inside surface and then capillary condensation occurred, leading to the shift of the reflectivity of the rugate PSi to longer wavelengths due to the increase in the refractive indices of the porous medium. The observed redshift was triggered by the increased average refractive indices of the porous medium was induced by the partial substitution of air by the organic liquid phase in the multilayer pores of rugate PSi due to the capillary condensation effect.

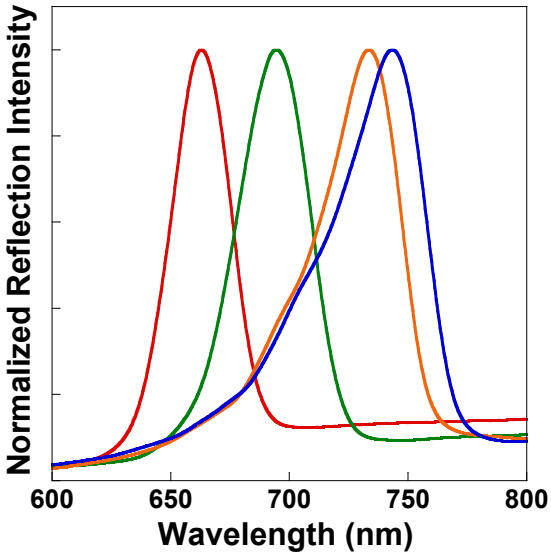

Figure 1.6. Reflection spectra of rugate PSi filters (red: λ = 663 nm) under a flux of toluene (green, λ=695 nm, Δλ= 32 nm), hexane (orange, λ=734 nm, Δλ = 71 nm), chloroform (blue, λ=744 nm, Δλ=81 nm).

The reflection shifts obtained for these organic substances are showed in Figure 1.6 as a function of their corresponding refractive indeces. An examination of the results showed that different organic species shown in Figure 1.7 result in different resonance shifts. However, even though the reflection redshift was triggered by the increase of a refractive index, it did not show a definite relationship with the refractive index of the analyte. Table 1 shows the refractive index data of the above analytes. For species having close values of refractive index, namely toluene and chloroform, the reflection peak shift can be distingguished well. In addition, higher refractive indeces do not necessarily translate to more prominent shifts; for example, toluene has a relatively higher refractive index, but was found to exhibit the smallest reflectivity redshifts. These results are very inconsistent with the reports that the reflection redshift exhibits a positive linear dependence on the refractive index[18-20]. This discrepancy can be due

to the fact that the redshift is dominated by not only the refractive index of organic substances, but also the percentage of filling fraction of the stratified silicon pores due to capillary condensation. Our previous work found that the PSi reflection shift range was directly dependent on the vapor pressure of organic molecules [20]. As shown in Table 1, the vapor pressure increases gradually for toluene, hexane, and chloroform. Based on the above results, the extent of the reflectivity redshift was affected by the vapor pressure of the organic solvents. The organic molecules are adsorbed on the inside surface of PSi and then undergo capillary condensation that changes the refractive index of the rugate PSi filters. The different extent of the reflection redshift generated due to the different concentration of organic solvents in carrier gas is due to the different filling fraction of the organic compound in the silicon pores.

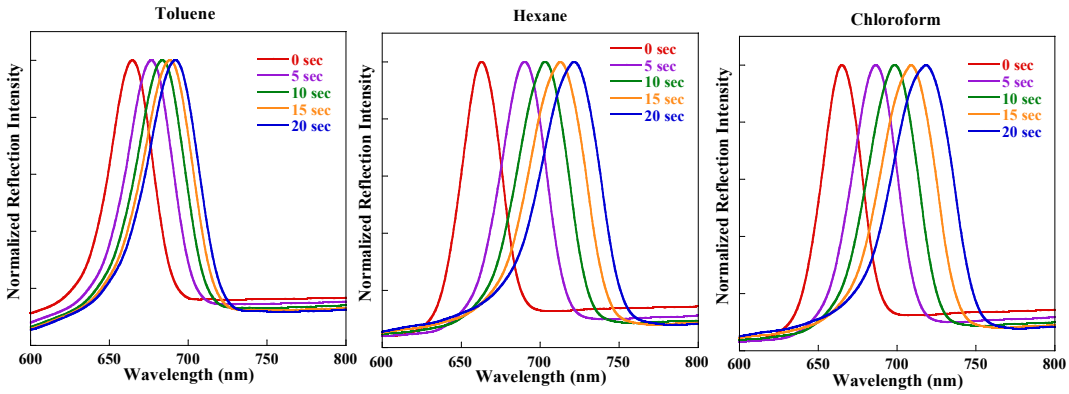

Figure 1.7. Reflection spectra of rugate PSi within 20 seconds under the same argon flow (1 SLM) for three different organic solvents.

Table 1. Physical parameters of toluene, hexane, and chloroform.

Organic Species	Toluene	Hexane	Chloroform
Refractive index	1.497	1.354	1.446
Dipole moment/D	0.36	0.08	1.15
Vapor Pressure/kPa	2.8	16.2	21.2

An examination of Figure 1.2 indicates that the PL quenching of rugate PSi filters is due to the organic solvent molecules that are physisorbed on the surface of the luminescent chromophore and then undergo capillary condensation inside the pores. Based on the observed sharp PL decrease in the presence of organic solvent vapor, we predict that rugate PSi filters will exhibit greater sensitivity than monolayer PSi with a broad PL peak. To investigate the PL quenching sensitivity behaviors of the organic vapor, an organic vapor sensor based on the observed sharp PL decrease in the presence of organic solvent vapor, we predict that rugate PSi filters will exhibit greater sensitivity than monolayer PSi with a broad PL peak. To investigate the PL quenching sensitivity behaviors of the organic vapor, an organic vapor sensor based on rugate PSi filters was fabricated and tested for different chemical vapor pressures of toluene, hexane, and chloroform. Figure1.8(A-C) showed a shift of the reflection of the rugate PSi to longer wavelengths due to the increase in the refractive indices of the porous medium.The steady-state PL spectra shown in Figure 1.8(D-F) displayed PL quenching under the exposure to the vapor pressure of the above three organic species. Organic vapor (carrier gas flow was 1 SLM) was injected into the surface of rugate PSi sample, resulting in reversible PL quenching. The PL intensity of the rugate PSi in vacuum can be recovered to that of the original spectrum.The PL intensities for different organic species vapors were decreased compared to the initial PL. However, the PL quenching magnitudes of the rugate PSi filters varied greatly and were 6.7%,

11.4%, and 52.7% within 20 seconds for toluene, hexane and chloroform, respectively. However, for monolayer PSi shown in Figure 1.8(G-I), the corresponding values were 5.1%, 9.5%, and 42.9%, respectively. These results indicated that the sharp PL peak of the rugate PSi filters is more sensitive than the broad PL of the monolayer PSi. The reflection showed that reflectivity peak redshifted by 27, 58, and 53 nm within 20 seconds. Even though the vapor pressure of chloroform was higher than that of hexane, the reflection redshift for chloroform was smaller than that for hexane.The PL wavelength redshifts were 17, 33, and 28 nm for toluene, hexane, and chloroform, respectively, within 20 seconds during sensing. The PL redshift of chloroform was also smaller than that of hexane.This result is due to the much smaller polarity of hexane compared to chloroform. Since the fresh porous silicon surface was hydrophobic, hexane adsorbed more easily on the pore surface of PSi.

Figure 1.3 shows that the PL was enhanced by reflection, and the PL and reflectance peaks were overlapped at the same wavelength position. The reflection and PL both redshifted during the organic solvents sensing, which might be due to the increase of refractive indices. However, the extent of the PL redshift was smaller than that of the reflection redshift, illustrating that the PL redshift is induced by the reflection redshift. This conclusion is also supported by the similar behavior of the reflection redshift and PL redshift during the first 5 seconds larger than the subsequent interval time of 5 seconds as shown in the upper half part of Figure 2.8, respectively.

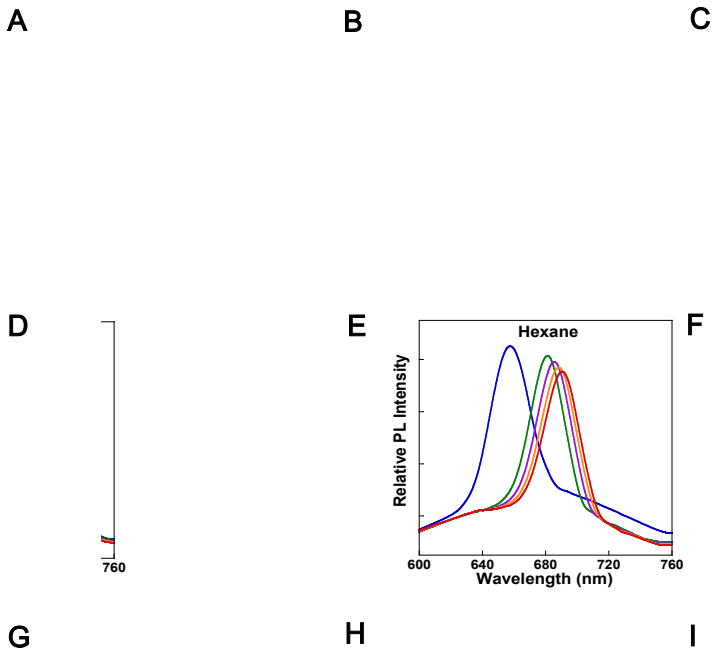

Figure 1.8. Reflection spectra (A, B, and C) and Time-resolved PL (D, E, and F) of rugate PSi and monolayer PSi (G, H, and I, only PL) under the exposure of different organic vapors with identical argon flow rate (1 SLM) for 20 sec.

In Figure 1.8, the PL of the monolayer PSi was blue-shifted by 30 nm when it was exposed to chloroform vapor but to a lesser extent for hexane (4 nm) and toluene (2 nm) vapors. Sailor reported that the PL wavelength was blue-shifted from 670 nm to 630 nm when PSi was exposed to tetrahydrofuran vapor [21]. These results may be

due to the faster PL emission decay of the monolayer PSi at the longer wavelengths, which was determined by different excited state lifetime for emission (τ) at different wavelength. Figure 1.9 showed different quenching rates of excited emission at 650, 700, and 750 nm for monolayer PSi under the exposure of chloroform vapor.

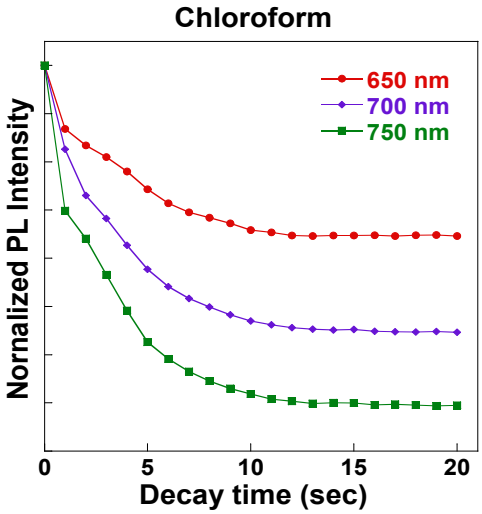

Figure 1.9. Time-resolved PL emission decays of monolayer PSi at different wavelengths under chloroform vapor exposure.

The left figure in Figure 1.10 shows a three-dimensional plot for the identification of the analyte using the relationship between the shifts in the PL wavelength, PL quenching, and the vapor pressure of three different organic substances. The rugate PSi was sensed 3 times of each species and 3 spheres that represent the results of the measurements are shown in the same color and connected by lines crowd together, forming a . A smaller area of the cluster indicates better reproducibility and reliability. The right figure in Figure 1.10 shows a three-dimensional plot used for the identification of the functional relationships between the quenching percentage of the normalized PL area, PL wavelength shift, and the sensing time of the three different analytes. The different directions of testing curves validate that toluene, hexane, and

chloroform can be clearly distinguished, which means that the volatile organic compounds detection using rugate PSi is specific and effective.

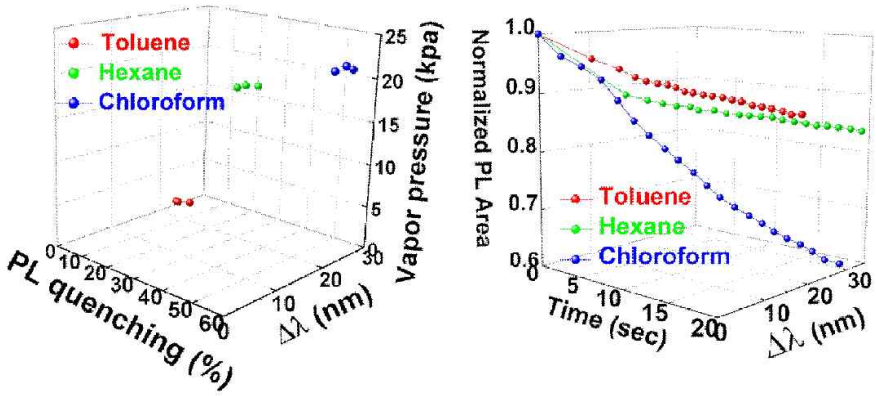

Figure 1.10. LEFT: 3-dimensional plot showing the relationship between the wavelength shift of the PL and PL quenching as a function of different vapor pressures of the three analytes. RIGHT: 3-dimensional plot revealing the relationship between the normalized PL area, the PL wavelength shift as a function of sensing time of the three analytes.

Previous work in our group has demonstrated that the dynamic Stern-Volmer quenching model shows linear relationships between PL quenching and quencher concentration for different analytes [21]. However, the Stern-Volmer constants for the different analytes were not identical. These result indicated that the PL quenching depended on not only the vapor pressure of the analytes, but also the functionalities of organic molecules. Additionally, Nayef et al. reported [22] that PL quenching is related to the dipole moment of organic molecules. This finding can be interpreted as being due to the stabilization of the PSi surface trap by the alignment of the dipoles of the

organic molecules. In the present study, the observed PL quenching of chloroform was much larger than that for hexane despite their similar vapor pressure, which should be attributed to the larger dipole moment of chloroform. However, the dipole moment of toluene is larger than that of hexane, but its PL quenching was smaller than hexane. This result is consistent with our previous reports that PL quenching depends on the vapor pressure. The reflectance results were affected by the vapor pressure and polarity of the analytes, and in turn, the polarity of the analyte depends on the dipole moment of organic molecules. Thus, both the analyte vapor pressure and dipole moment are important factors for PL quenching used as the basis for volatile organic compounds detection.

1.4. Conclusion

A preparation of rugate PSi filters exhibiting enhanced PL through the constructive overlap with reflectivity was reported. The PL changes were used for the detection of different volatile organic compounds with different vapor pressures and dipole moments. The reflectivity redshift and PL quenching of rugate PSi were both affected by the vapor pressure and dipole moment of the organic compounds. It is concluded that rugate PSi filters can be considered for use in chemical vapor sensors based on the reflectivity redshift and PL quenching.

1.5. References

[1] Canham, L. T. Silicon quantum wire array fabrication by electrochemical and chemical dissolution of waferd. Appl. Phys. Lett. 2019, 57, 1046-1048.

[2] Hirschman, K. D.; Tsybeskov, L.; Duttagupta, S. P.; Fauchet, P. M. Silicon-based visible light-emitting devices integrated into microelectronic circuits. Nature 1996, 384, 338-341.

[3] Sohn, H.; Letant, S.; Sailor, M. J.; Trogler, W. C. Detection of fluorophosphonate nerve warfare agents with a porous silicon interferometer. J. Am. Chem. Soc. 2000, 122, 5399-5400.

[4] Jenie, S. A.; Plush, S. E.; Voelcker, N. H. Recent advances on luminescent enhancement-based porous silicon biosensors. Pharm. Res. 2016, 33, 2314-2336.

[5] Wang, J.; Kumeria, T.; Bezem, M. T.; Wang, J.; Sailor, M. J. Self-reporting photoluminescent porous silicon microparticles for drug delivery. ACS Appl. Mater. Inter. 2018, 10, 3200-3209.

[6] Gu, L.; Hall, D. J.; Qin, Z.; Anglin, E.; Joo, J.; Mooney, D. J.; Howell, S. B.; Sailor, M. J. In vivo time-gated fluorescence imaging with biodegradable luminescent porous silicon nanoparticles. Nat. Commun. 2013, 4, 2326.

[7] Kim, H. J.; Kim, Y. Y.; Lee, K. W. Sensing characteristics of the organic vapors according to the reflectance spectrum in the porous silicon multilayer structure. Sensor. Actuat. A-Phys. 2011, 165, 276-279.

[8] Ali, N. K.; Hashim, M. R.; Aziz, A. A. Effects of surface passivation in porous silicon as H2 gas sensor. Solid Sotate Electron. 2008, 52, 1071-1074.

[9] Rittersma, Z. M.; Splinter, A.; Bödecker, A.; Benecke, W. A novel surface-micromachined capacitive porous silicon humidity sensor. Sensor. Actuat. B-Chem. 2000, 68, 210-217.

[10] Ben-Chorin, M.; Kux, A. Adsorbate effects on photoluminescence and electrical conductivity of porous silicon. Appl. Phys. Lett. 1994, 64, 481-483.

[11] Curtis, L. C.; Doan, V. V.; Credo, G. M.; Sailor, M. J. Observation of optical cavity modes in photoluminescent porous silicon films. J. Electrochem. Soc. 1993, 140, 3492-3494.

[12] Lauerhaas, J. M; Sailor, M. J. Chemical modification of the photoluminescence quenching

of porous silicon. Science. 1993, 261, 1567-1568.

[13] Zicheng, Z.; Honglae Sohn. A Novel Chemical Gas Vapor Sensor Based on Photoluminescence Enhancement of Rugate Porous Silicon Filters. Sensors. 2020, 20, 2722.

[14] Hiller, D.; López-Vidrier, J.; Gustch, S.; Zacharias, M.; Wahl, M.; Bock, Wolfgang.; Brodyanski, A.; Kopnarski, M.; Nomoto, K.; Valenta, J.; Kongig, D. Boron-incorporating silicon nanocrystals embedded in SiO2: Absence of free carriers vs. B-induced defects. Sci. Rep. 2017, 7, 1-11.

[15] Park, M. A.; Sohn, H. Fabrication and optical characterization of Bragg resonance luminescence porous silicon. Semicond. Sci. Technol. 2015, 31, 014013-014018.

[16] Cho, B.; Jin, S.; Lee, B. Y.; Hwang, M.; Kim, H. C.; Sohn, H. Investigation of photoluminescence efficiency of n-type porous silicon by controlling of etching times and applied current densities. Microelectron. Eng. 2012, 89, 92-96.

[17] Lee, S. G.; Koh, Y.; Kim, J.; Woo, H. G.; Kim, S.; Sohn, H. Chemical sensor based on porous silicon dual transducers. J. Nanosci. Nanotechnol. 2010, 10, 3266-3270.

[18] Huanca, D. R.; Ramirez-Fernandez, J.; Salcedo, W. J. Porous silicon optical cavity structure applied to high sensitivity organic solvent sensor. Microelectronics. J. 2008, 39, 499-506.

[19] DeLouise, L. A.; Kou, P. M; Miller, B. L. Cross-correlation of optical microcavity biosensor response with immobilized enzyme activity. Insights into biosensor sensitivity. Anal. Chem. 2005, 77, 3222-3230.

[20] Jang, S.; Koh, Y.; Kim, J.; Park, J.; Park, C. Kim, S. J.; Cho, S.; Ko, Y. C.; Sohn, H. Detection of organophosphates based on surface-modified DBR porous silicon using LED light. Mater. Lett. 2008, 62, 552-555.

[21] Ahn, J.; Cho, B.; Kim, S.; Sohn, H. Detection of organic vapors based on photoluminescent Bragg-reflective porous silicon interferometer. J. Nanosci. Nanotechnol. 2015, 15, 4999-5003.

[22] Lauerhaas, J. M.; Credo. G. M.; Heinrich. J. L.; Sailor, M. J.; Reversible luminescence quenching of porous Si by solvents. Mat. Res. Soc. Symp. Proc. 1992, 256, 137-141.

[23] Nayef, U. M.; Hussein, H. T. Abdul Hussein, A. M. Study of photoluminescence quenching in porous silicon layers that using for chemical solvents vapor sensor. Optik. 2018, 172, 1134-1139.

Part 2

Enhanced Detection of Organic Vapors Based on Photoluminescent Distributed Bragg-Reflective Porous Silicon Interferometer

2.1. Introduction

PSi has been attracted widely attention for a variety of applications including drug delivery system [1], medical diagnostics [2], chemical and biological sensors [3,4], etc, because of its photo- and electro-luminescence characteristics [5, 6]. PSi is also an ideal functional material used in sensing applications for gas and liquid due to its sponge-like structure. It has a high surface to volume ratio with various orientation of pores and pore diameters that can be altered during production [7, 8]. The main sensing techniques have been researched to achieve signal transduction including capacitance [9], resistance [10], reflectivity [11], and PL [12].

Typically, PSi fabricate by p-type silicon wafer under dark condition exhibits well-defined Fabry-Perot fringes in the optical reflectivity spectrum. The condensation of sensing molecules, such as nerve agents [13, 14], organic solvents [15, 16], DNA [17], and proteins [18, 19], in the pores can lead to reflection peak redshift due to a change in the refractive index of the PSi. However, superior luminescent PSi samples can be prepared by a galvanostatic photoetch of highly doped n-type silicon wafer under illumination.In our previous work, a type of rugate PSi which having both of reflection and PL was successfully prepared by sinusoidal current under illumination[20]. To the best of our knowledge, this light emission most likely results from quantum confinement effects within silicon quantum dots.

PL efficiency of PSi depends on its interior structure and surface properties [21]. Vapors of different volatile organic compounds have been sensed by PL quenching based on organic molecules having different functionalities [22]. Here, a novel preparation method about PSi DBR is reported which exhibiting both well-defined Bragg reflection and superior PL by n++-typesiliconwafers.PLisenhanced and narrowed due to constructive propagation of reflection from PSi. Organic vapor of toluene, hexane, and chloroform have been detected by PL quenching of PSi DBR.

2.2. Experiments

2.2.1. Materials

n++-type (0.001 ~ 0.003 Ω•cm) and n-type (1 ~ 10 Ω•cm) single-side polished <100> oriented silicon wafer (Prime grade, Siltronix Inc., Archamps, France),HF (48 – 51%, ACS Reagent, J.T. Baker, PA, USA), ethanol (99.8%, Merck, Darmstadt, Germany), toluene (99.5%, ACS reagent, Aldrich Chemicals, Sigma-Aldrich, Steinheim, Germany), hexane (95%, ACS reagent, Aldrich Chemicals, Sigma-Aldrich, Steinheim, Germany), and chloroform (>99.5%, ACS reagent, Aldrich Chemicals, Sigma-Aldrich, Steinheim, Germany) were used as received.

2.2.2. Preparation of DBR PSi

PSi DBR samples were prepared via electrochemical etching based on n++-type (0.001 ~ 0.003 Ω•cm) single-side polished <100> oriented silicon wafer (Prime grade, Siltronix Inc., Archamps, France). The silicon wafer as the anode and a Pt ring as the cathode were arranged in Teflon cell, using a mixed solution of volume ratio of 48 wt% aqueous HF (Anhydrous,Sigma-Aldrich,Germany) and absolute ethanol (Anhydrous, Sigma-Aldrich, Germany) is 1:1 as etching electrolyte at room temperature. The etching current was supplyed by a high-precision constant current equipment (Keithley 2420, Keithley Instruments Inc., Cleveland, OH, USA). Low porosity layers (L) were obtained by 31 mA/cm2for 4.2 s and high porosity layers (H) of porosity were obtained by a current density of 320 mA/cm2for1.14 s. An etch-stop step of zero current was applied for 2s after each formation for the regeneration of HF concentration. The “L” and “H” layers were periodically repeated 80 times to form PSi DBR. Galvanostatic etching was performed under illumination with a 300 W tungsten filament bulb for the etching duration. Samples were rinsed by ethanol several times and dried with argon gas flow before usage.

2.2.3. Instruments and Data Acquisitions

Steady-state PL spectra were obtained with an Ocean Optics S2000 spectrometer fitted with a fiber optic probe. The excitation source was a LED (λmax = 460 nm) focused on the sample (at a 45° angle to the normal of the surface) by means of a separate fiber. Light was collected at a vertical direction to the surface of PSi samples with a fiber optic. Spectra were recorded with a CCD-detector in the wavelength range of 400 –900 nm. Values of percent quenching are reported as $(I_0\text{-}I)/I_0$, where I_0 is the initial intensity of the luminescence of PSi DBR, integrated between 400 and 900 nm, in the absence of quencher and I is the integrated luminescence intensity of PSi DBR in the presence of analytes. Interferometric reflectance spectra of PSi DBR samples were measured by using an Ocean Optics S2000 spectrometer. A tungsten light source was focused onto the center of a PSi DBR surface. Spectra were recorded with a CCD detector in the wavelength range of 400–1200 nm. The illumination of the surface as well as the detection of the reflected light was performed along an axis coincident with the surface normal. Measurements were performed at least three times for each analyte studied. The morphologies of PSi DBR were obtained by cold field emission scanning electron microscopy (FE-SEM, S-4800, Hitachi, Ltd., Chiyoda, Tokyo, Japan).

2.2.4. Characterization

Morphologies of PSi samples were obtained by a cold field emission scanning electron microscopy (FE-SEM, S-4800, Hitachi).

2.2.5. Detection of Organic Vapor

The effectiveness of the amplified PL in regards to detection performance by PSi DBR was examined by sensing organic solvents. The results of organic vapor detection performance by PSi DBR were compared with monolayer PSi. The PSi DBR were placed in an exposure chamber fitted with an optical window, and toluene, hexane, and

chloroform were used to investigate the adsorption behavior. Argon gas was used as the carrier gas for the volatile organic compound vapors, and the chemical vapor concentration was adjusted by the flow meters. The influence of different organic species vapors namely, toluene, hexane, and chloroform on the PL spectra of PSi DBR were studied. All sensing measurements were carried out at room temperature. The PL of PSi DBR and monolayer PSi samples were measured in the presence of different organic species with various vapor concentrations at the same carrier gas flow. Optical reflection spectra were measured using a tungsten–halogen lamp and a CCD spectrometer fitted with a fiber optic input. Figure 1.1 showed the schematic diagram of the gas measuring system.

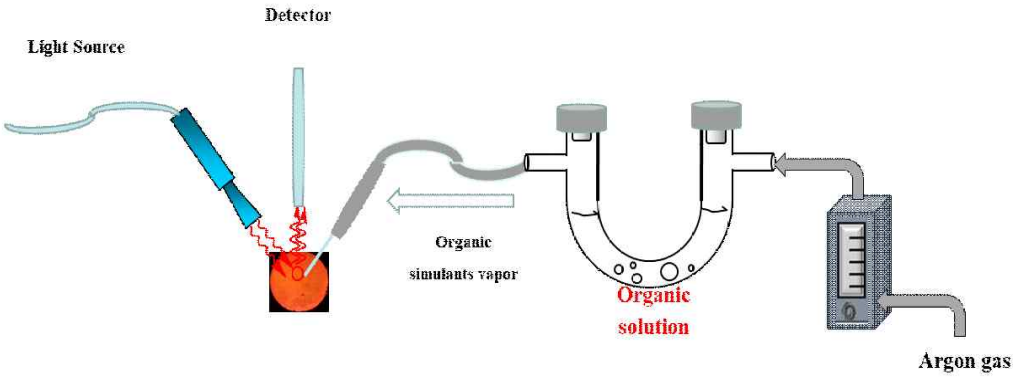

Figure 1.1. Schematic diagram of the gas measuring system

2.3. Results and Discussion

PSi DBR exhibiting both Bragg reflection and PL was successfully fabricated by applying square current waveform with a 300 W tungsten filament bulb for illumination in the etching duration. Photographs of PSi DBR are shown in Figure 2.2 A Bragg reflector is a structure which consists of an alternating sequence of layers made of two different porosities. A Bragg reflector exhibits a high reflectivity band with a Bragg wavelength, lBragg, depending on the thickness of the layers (L_1,L_2) and the corresponding refractive indices (n_1,n_2). The reflectivity is determined by the refractive index contrast Δn between the layers and number of layer pairs. The Bragg reflector is characterized by its central wavelength λ_0 (at normal incidence) and by the reflection bandwidth $\Delta\lambda$, which is determined mainly by the index contrast.

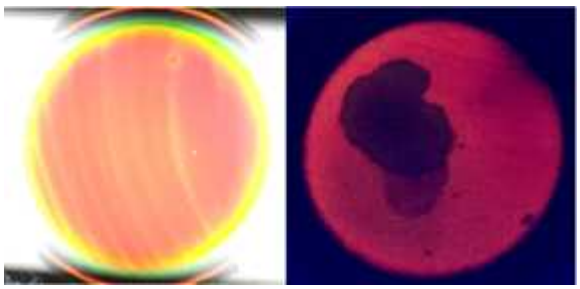

Figure 2.2. Images of PSi DBR sample under white light (left) and UV light(right). Dark area in the right picture represents PL quenching by hexane.

Figure 2.3 shows the FE-SEM images of the morphology of the top surface, cross-section of PSi DBR, and rugate PSi which prepared and researched before. FE-SEM image (A) of PSi DBR shows that the PSi prepared with 80 repeats exhibited very stable and flat surface with pore sizes between 10–20 nm. Cross section images(B and E) showed in the middle(top and bottom) indicate the depth of PSi DBR layers is

29.6μm, is much smaller than rugate PSi(88.5μm).The partial enlarged detail of cross-sectional image(C and F) shows that the PSi DBR has distinct and alternating PSi layers structures, which was consistent with alternating etching currents and the responses of different apertures of porous silicon layers. However, the weeny stripe structure of the rugate PSi sample represent gradually varied with the sine-shape porous layers which was due to sinusoidal current density. On the micro scale, the change of PSi DBR structure between adjacent layers is larger than rugate PSi.

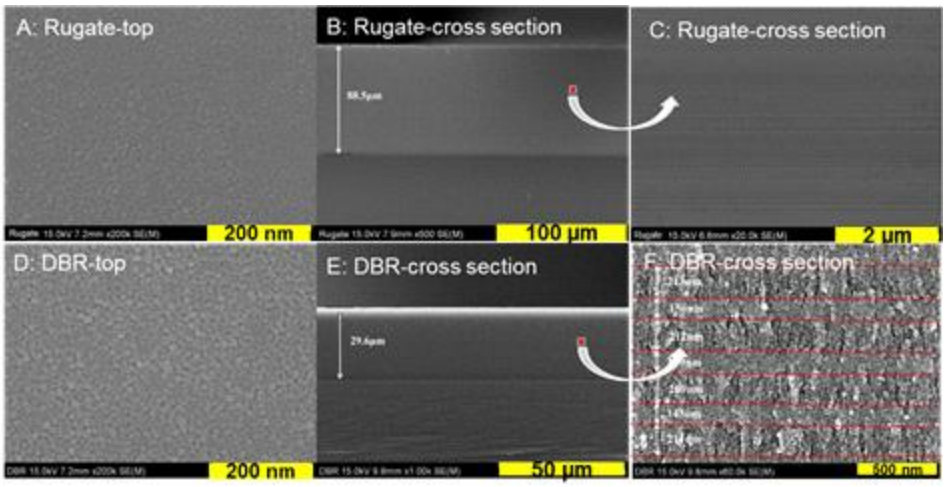

Figure 2.3. Morphology of surface and cross-section of PSi DBR (A,B,C) and rugate PSi (D,E,F) were shown by SEM.

Reflection and PL shown in Figure 2.4 were measured to investigate the optical properties of PSi DBR. Surprisingly, PSi DBR displayed PL and reflection are both sharp at the same wavelength position of 683 nm FWHM of 25 nm. Then, the PL of PSi DBR was due to the quantum confinement of silicon nanocrystallites, and the overlap of reflection and PL enhanced the PL intensity. In the contrast, the intensity of PSi DBR was stronger than rugate PSi sample, and the PL of rugate PSi overlapped

with reflection at 663nm.

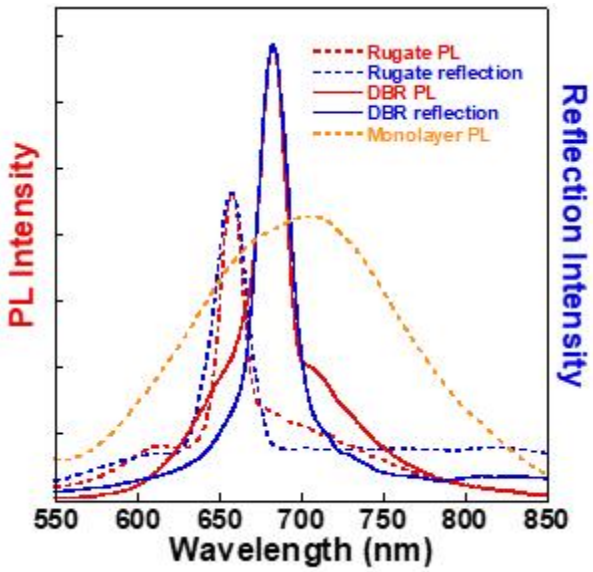

Figure 2.4. PL (PSi DBR: red solid line, Rugate: red dotted line, Monolayer:orange dotted line) and reflection(PSi DBR: blued solid line, Rugate: blue dotted line) spectra of PSi DBR, rugate and monolayer PSi.

The PSi DBR is a structure of alternating varied PSi layers, which consists of high and low porosities. The PSi DBR exhibits a high reflection band wavelength, depending on the periodic varying PSi layers and the corresponding refractive indices, thus, the reflectivity is collected by the several alternating varied PSi DBR layers and refractive

index between the alternating layers. The rugate PSi has similar result with PSi DBR, however, the monolayer PSi quantum dots that have vertical cylindrical cavities but lack reflection peak features. For PL, the narrow PL peak of PSi DBR is due to the quantum confinement of silicon quantum dots in special porous silicon structure, as shown in Figure 2.5(A,B and C). The right half of Figure 2.5 displays the PL of PSi quantum dots sharply narrowed and amplified by the repeated multilayer(PSi DBR and rugate) PSi structure compared to the monolayer PSi. Furthermore, the PL intensity of PSi DBR was stronger than rugate PSi maybe due to the featured structure of PSi DBR embodied more effective behavior of quantum confinement for silicon quantum dots than rugate PSi sample.

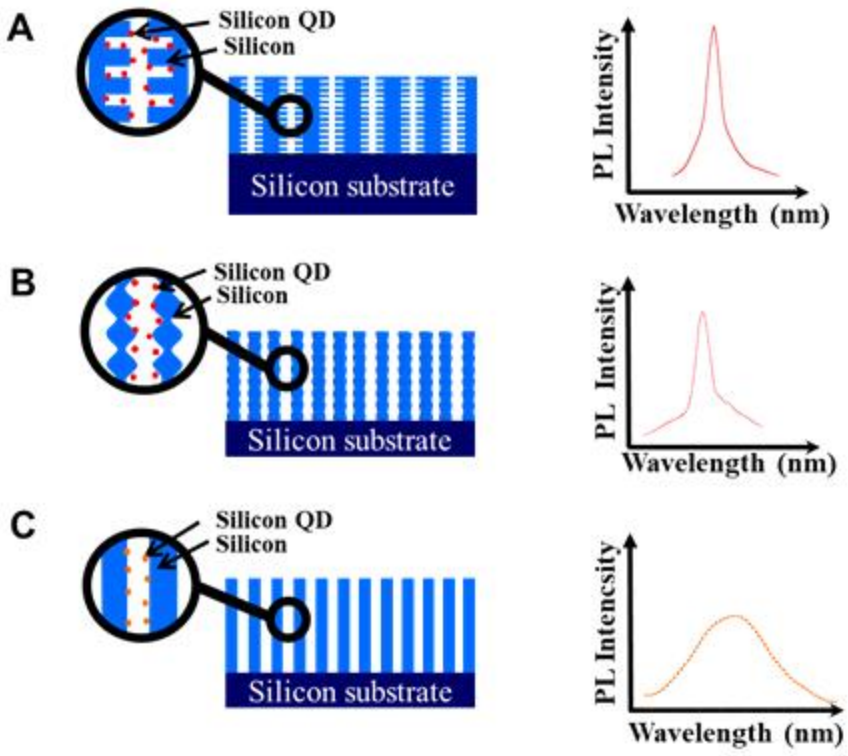

Figure 2.5. Simulated structure diagram of (A) PSi DBR, (B) rugate PSi and (C) monolayer PSi. The right half shows PL spectra of PSi DBR (red solid line), rugate PSi (red dotted line) and monolayer PSi (orange dotted line).

As shown in Figure 2.6, adsorption of organic vapors and capillary condensation in the pores cause thereflectionofthePSi DBR to shift to longer wavelengths owing to the increase for refractive indices of the porous medium. Overall, the redshift was caused by the increased average efractive indices of the porous medium that are the result of a partial space in the multilayer pores was occupied by organic liquid phase in PSi DBR due to the capillary condensation effect.

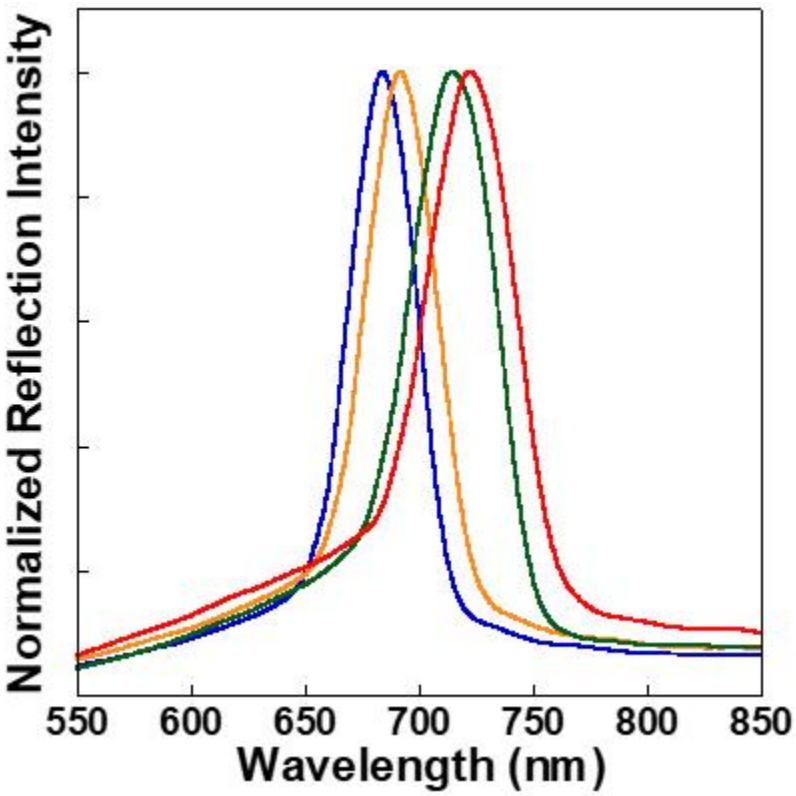

Figure 2.6. Initial reflection spectra of fresh PSi DBR (blue: λ= 683 nm) and PSi DBR under a flux of toluene (orange, λ = 691 nm, Δλ = 8 nm), hexane (green, λ= 706 nm, Δλ = 23 nm), chloroform (red, λ =721 nm, Δλ =38 nm).

The reflection shifts obtained for these organic substances shown in Figure 2.6 result in resonant shifts with different extents. However, although a red shift was caused by the increase of a refractive index in porous matrix, it did not follow a clear relationship with the refractive index of the organic solvents. This fact may comes down that the average refractive indices of the porous medium is dominanted by both of fillng fraction in stratified silicon pores and the refractive index of organic liquid analytes. Our previous work reported that the reflection redshift mainly depended on the vapor pressure of analytes, not the functionalities of the organic molecules for monolayer PSi [23]. As shown in Table 2, the vapor pressure of toluene, hexane, and chloroform are 2.8 kPa, 16.2 kPa, and 21.2 kPa, respectively. This work are consistent with previous reports.

Table 2: Physical parameters of 3 organic solvents

Organic species	Toluene	Hexane	Chloroform
Refractive index	1.50	1.35	1.45
Dielectric constant	2.38	1.93	4.81
Vapor Pressure/kPa	2.8	16.2	21.2

As it was showed in Figure 5, the reflection of PSi DBR redshifted for different extent of 8nm, 23nm and 38nm for toluene,hexane and chloroform at saturation condition. However, in our previous work, the reflection of rugate PSi redshifted 32nm, 71nm and 81nm for toluene, hexane and chloroform. This means that the extent of

reflection redshift of rugate PSi are larger than PSi DBR. In fact, the extent of reflection redshift was affected by porosity of PSi samples due to reflection redshift is triggered by the increase of refractive indice of porous media. The porosity of PSi DBR and rugate PSi were measured via a gravimetric method [24], shown in following formula:

$$P = \frac{(m_1 - m_2)}{(m_1 - m_3)} = \frac{V_{voids}}{V_{layer}} (\times 100\%)$$

The Silicon wafer was weighted before etching (m_1),after etching(m_2) and after total removal of the PSi layer by dissolution in NaOH solution(m_3). The porosity of PSi DBR and rugate PSi were 57.5% and 64.9%, respectively. Because the porosity of PSi DBR was larger than rugate PSi, it can be well explained the extent of PSi DBR of reflection redshift was smaller than rugate PSi.

Figure 2.7(A,B,C) showed the shift of the real reflection of PSi DBR to longer wavelengths due to the increase in the refractive indices of the porous medium. Hexane is nonpolar, toluene is weak polar, and chloroform having a bigger polarity. However, the surface of fresh PSi ishydrophobic, the vapor of hexane and toluene were easy adsorbed on the PSi surface and then capillary condensation occured. Figure 2.7(A, B) showed it seemed that the reflectivity peak of PSi reached the equilibrium at the beginning after touched hexane and toluene. However, the reflection for chloroform needed a longer time to reach the equilibrium due to polar substance was more hard adsorbed on the hydrophobic PSi surface. Hence, the chloroform molecules was forced went through the pores because its concentration is bigger in the carrier gas(having bigger vapor pressure). The intensity of following reflection spectra were higher than initial because the surface of PSi and the angle of incident and reflected rays changed that was caused by different volume of solvent liquid was occupied the space of pores. The increased extent of reflection spectra for toluene was smallest due to only a small

partial space of pores were occupied by toluene liquid because of vapor pressure is very small.

The reflection redshift by 8, 27, and 31nm within 10s for toluene, hexane, and chloroform; In contrast, PL redshift showed in Figure 2.7(D,E,F) were 12, 25, and 27nm, respectively. The order of PL redshift and reflection shift are the same from toluene, hexane, and chloroform, which indicated the PL shift and reflection shift maybe due to the same mechanism that about the increase of refractive indices of the porous medium.

The organic solvent molecule was physisorbed on the surface of luminescent chromophore in PSi DBR and then capillary condensation occurred inside the pores resulting in PL quenching. To investigate the PL quenching behavior of organic vapor sensing, organic vapor sensor has been conducted by PSi DBR with different chemical vapors of toluene, hexane, and chloroform. The steady-state PL spectra shown in Figure 2.7(D,E,F) displayed PL quenching under the exposure of different organic vapors. Organic vapor (massflow1SLM) was injected on the samples surface resulting inreversible PLquenching. The PL intensity of the samples spectra in vacuum can be recovered to the initial spectrum.

The PL intensity for different organic solvents vapors decreased compared to the original PL. However, the PL quenching varied greatly within 10s. As shown in Figure 2.7(D,E,F), the magnitudes of PL quenching were 35%, 50%, and 90% for toluene, hexane, and chloroform within 10s respectively. The photographs in Figure 2.7(G,H,I) showed the comparison of different PL quenching effect for sample of rugate PSi based on three organic chemical solvent vapors. The magnitudes of PL quenching were 6.7%, 11%, and 53%for toluene, hexane, and chloroform within 20s respectively. However, the corresponding values were 5.1%, 9.5%, and 42.9% for monolayer PSi. This work and the research of rugate PSi demonstrated the sharp PL with narrow FWHM were more sensitive than broad PL of monolayer PSi used in detection of organic vapor. Furthermore, the PL quenching magnitude of PSi DBR was larger than rugate PSi for

all the aforementioned organic chemical solvents. These results indicated the PL with stronger intensity of PSi DBR was more sensitive than rugate PSi.

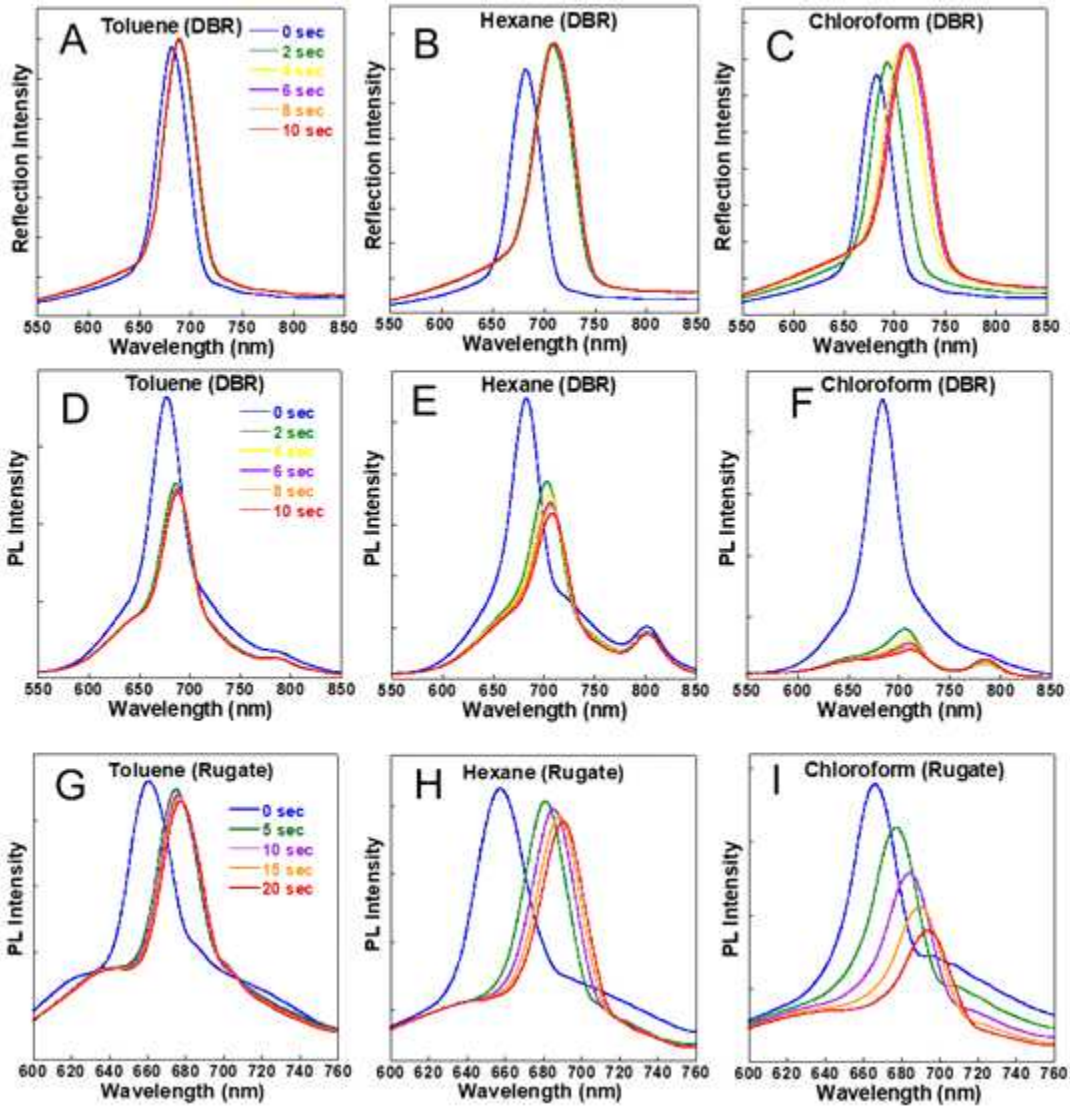

Figure 2.7. Reflection redshift(A,B,C) and time-resolved PL of PSi DBR (D, E, F) for 10 seconds and rugate PSi (G, H, I) for 20 seconds under the exposure of different organic vapors with identical argon flow rate (1 SLM).

The reflection redshift, PL redshift and the extent of PL-quenching at the beginning (the first 2 seconds) was considerably larger than the following sensing time. These results indicate the detection application of VOCs base on PL quenching and reflection redshift of PSi DBR provide extremely high sensitivity and ultra-fast response. Figure 2.7 showed reflection shift(A,B,C) and PL quenching(D,E,F) almost reached saturation at 10 seconds under the exposure of organic vapor. However, the rugate PSi couldnot reach saturation within 20 seconds. These results canbe explained by 2 factors which including the depth of rugate PSi(88.5μm) were much bigger than PSi DBR(29.6μm) and the porosity of rugate PSi (64.9%) were bigger than PSi DBR(57.5%). The much larger pore volume resulted in capillary condensation of organic vapor in rugate PSi need more time. Therefore, PSi DBR are more sensitive and quick than rugate PSi used for VOCs detection based on optical performance.

The previous report in our group has already confirmed the dynamic Ster-Volmer quenching model which showed straight lines between extent of PL quenching and quencher concentration, but Stern-Volmer constants varied greatly for different analytes [23]. These research indicated that the PL quenching of PSi were affected not only the vapor pressure of solvents, but also some physical properties of organic molecules. Fellah and Juraj Dian [25, 26] reported the positive correlation between PL quenching and dielectric effect of organic solvents. The dielectric constant is the main macroscopic physical quantity that comprehensively explained the internal dipole behavior of the medium. The positive correlation between PL quenching with the dipole moment or dielectric constant of the organic species are essentially identical. Though the dielectric constant of hexane is smaller than toluene, however, the PL quenching of hexane was larger than toluene. Our results further indicated that the PL quenching of PSi DBR

was affected by the vapor pressure of analyte.

Figure 2.8 showed the three-dimensional plot to specify the analyte using the relationship between the PL quenching, peak shifts of PL and vapor pressure of three research objects. The PSi DBR was exposed thrice under each analyte. Three same color globules connected by line, came together and formed a cluster. Smaller the area of the cluster, better is the reproducibility and reliability.

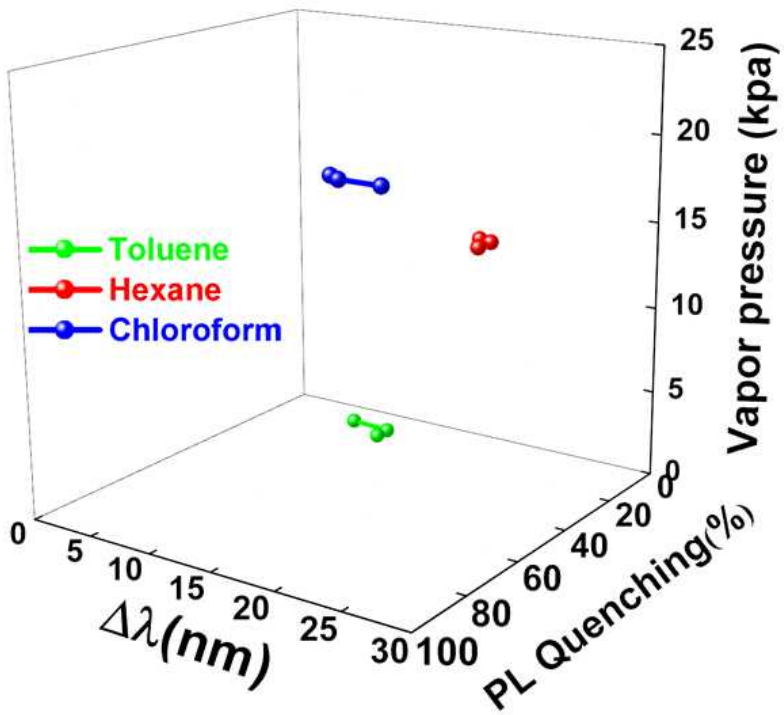

Figure 2.8. 3D plot showing the relationship between the PL shift (Δλ) and PL quenching as a function of different vapor pressures of three analytes such as toluene (green), hexane (red), and chloroform (blue).

Figure 2.9 showed the three-dimensional plot to specify the specifity relationships between the PL peak shift, the quenching percentages of normalized PL area and the sensing time of three analytes. The testing curves in different directions validating toluene, hexane, and chloroform are clearly differentiated from each other, which imply that the organic chemical solvent vapor detection by PSi DBR was specific and effective.

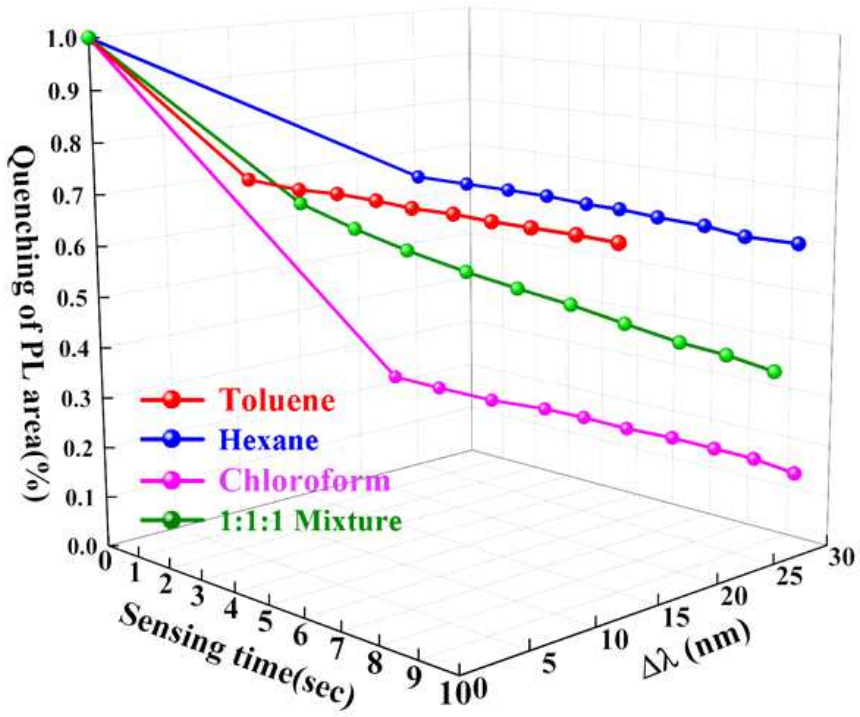

Figure 2.9. 3D plot showing the relationship between the PL peak shift(Δλ), normalized PL area and sensing time of three analytes such as toluene (green), hexane (red), and chloroform (blue).

2.4. Conclusion

A preparation of PSi DBR exhibiting enhanced PL through constructive overlaying with reflectivity was reported. The PL quenching and reflectivion redshift have been used for the detection of volatile organic compounds having different functionalities. Reflection redshift was mainly affected by the vapor pressure while the PL quenching was affected by dielectric constant and vapor pressure of the organic solvent. It is possible to conclude that PSi DBR structure of PSi can be considered as a chemical vapor sensor based on PL quenching and reflectivity redshift.

2.5. References

[1] J. Wang, T. Kumeria, M.T. Bezem, J. Wang, M.J. Sailor, Self-reporting photoluminescent porous silicon microparticles for drug delivery, ACS Appl. Mater. Inter. 10(2018) 3200-3209.

[2] T. Tieu, M. Alba, R. Elnathan, A. Cifuentes-Rius, N.H, Voelcker, Advances in porous silicon‐based nanomaterials for diagnostic and therapeutic applications, Adv. Therap. 2018, 1800095.

[3] V.Mulloni,L. Pavesi, Porous silicon microcavities as optical chemical sensors, appl. Phys. Lett. 76(2000), 2523-2525.

[4] F. A. Harraz, Porous silicon chemical sensors and biosensors: A review, Sens. Actuators, B, 202(2014) 897-912.

[5] L.T. Canham, Silicon quantum wire array fabrication by electrochemical and chemical dissolution of wafers, Appl. Phys. Lett. 57(1990) 1046-1048.

[6] K. Hirschman, L. Tsybeskov, S. Duttagupta, P. Fauchet, Silicon-based visible light-emitting devices integrated into microelectronic circuits, Nature, 384(1996) 338-341.

[4] K. Hirschman, L. Tsybeskov, S. Duttagupta, P. Fauchet, Silicon-based visible light-emitting devices integrated into microelectronic circuits, Nature, 384(1996) 338-341.

[5] J. Wang, T. Kumeria, M.T. Bezem, J. Wang, M.J. Sailor, Self-reporting photoluminescent porous silicon microparticles for drug delivery, ACS Appl. Mater. Interfaces, 10(2018) 3200-3209.

[6] L. Gu, D.J. Hall, Z.T. Qin, E. Anglin, J. Joo, M.David J, H. Stephen B, M.J. Sailor, In vivo time-gated fluorescence imaging with biodegradable luminescent porous silicon nanoparticles, Nat. Commun. 4 (2013) 1-7.

[7] P. Kumar, P. Huber, Effect of etching parameter on pore size and porosity of electrochemically formed nanoporous silicon, J. Nanomater.2007(2007) 89718.

[8] K. A. Kilian, A. Kilian, T. Bocking, J. J. Gooding, The importance of surface chemistry in nanostructured materials: lessons from mesoporous silicon photonic biosensors, Chem. Commun., 630(2009) 630-640.

[9] Z.M. Rittersma, A. Splinter, A. Bödecker, W. Benecke, A novel surface micromachined capacitive porous silicon humidity sensor, Sens. Actuators B Chem. 68 (2000) 210-217.

[10] M. Ben-Chorin, A. Kux, I. Schechter, Adsorbate effects on photoluminescence and electrical conductivity of porous silicon, Appl. Phys. Lett. 64(1994) 481-483.

[11] V. Mulloni, L. Pavesi, Porous silicon microcavities as optical chemical sensors, Appl. Phys. Lett., 76(2000) 2523-2525.

[12] S. Content, W.C. Trogler, M.J. Sailor. Detection of Nitrobenzene, DNT, and TNT Vapors by Quenching of Porous Silicon Photoluminescence, Chem Eur.J. 6(2000) 2205-2213.

Lauerhaas, M.J. Sailor, Chemical modification of the photoluminescence quenching of porous silicon, Science, 261(1993) 1567-8.

[13] S. Jang, J. Kim, Y. Koh, Y.C. Ko, H.-G. Woo, H. Sohn, Multi-encoded rugate porous silicon as nerve agents sensors, J. Nanosci. Nanotechnol. 7(2007) 4049-52.

[14] S. Jang, Y. Koh, J. Kim, J. Park, C. Park, S.J. Kim, et al., Detection of organophosphates based on surface-modified PSI DBR porous silicon using LED light, Mater. Lett. 62(2008) 552-555.

[15] P. Snow, E. Squire, P.S.J. Russell, L. Canham, Vapor sensing using the optical properties of porous silicon Bragg mirrors, J. Appl. Phys. 86(1999)1781-1784.

[16] S.G. Kim, S. Kim, Y.C. Ko, S. Cho, H. Sohn, PSI DBR-structured smart particles for sensing applications, Colloid Surf. A-Physicochem. Eng. Asp. 313(2008) 398-401.

[17] V.S.-Y. Lin, K. Motesharei, K.-P.S. Dancil, M.J. Sailor, M.R. Ghadiri, A porous silicon-based optical interferometric biosensor, Science, 278(1997) 840-843.

[18] K.-P.S. Dancil, D.P. Greiner, M.J. Sailor, A porous silicon optical biosensor: detection of reversible binding of IgG to a protein A-modified surface, J. Am. Chem. Soc. 121(1999) 7925-7930.

[19] S. Jang, J. Kim, Y. Koh, J. Park, H.-G. Woo, S. Kim, et al., Fabrication and Characterization of Surface-Derivatized Porous Silicon, J. Nanosci. Nanotechnol. 8(2008) 5166-5171.

[20] Z. Zhou, H. Sohn. A Novel Chemical Gas Vapor Sensor Based on Photoluminescence

Enhancement of Rugate Porous Silicon Filters, Sensors, 20, (2020) 2722.

[21] B. Cho, S. Jin, B.-Y. Lee, M. Hwang, H.-C. Kim, H. Sohn, Investigation of photoluminescence efficiency of n-type porous silicon by controlling of etching times and applied current densities, Microelectron. Eng. 89(2012) 92-96.

[22] U.M. Nayef, I. M. Khudhair, Synthesis of gold nanoparticles chemically doped with porous silicon for organic vapor sensor by using photoluminescence, Optik. 154(2018) 398-404.

[23] J. Ahn, B. Cho, S. Kim, H. Sohn, Detection of Organic Vapors Based on Photoluminescent Bragg-Reflective Porous Silicon Interferometer, J. Nanosci. Nanotechnol.15(2015) 4999-5003.

[24] P. Elia, E. Nativ-Roth, Y. Zeiri, Z.'e. Porat. Determination of the average pore-size and total porosity in porous silicon layers by image processing of SEM micrographs, Microporous Mesoporous Mater. (2016), doi: 10.1016/j.micromeso.2016.01.007.

[25] S. Fellah, R. Wehrspohn, N. Gabouze, F. Ozanam, J.-N. Chazalviel, Photoluminescence quenching of porous silicon in organic solvents: evidence for dielectric effects, J. Lumines. 80(1998) 109-113.

[26] J. Dian, T. Chvojka, V. Vrkoslav, I. Jelínek, Photoluminescence quenching of porous silicon in gas and liquid phases‐the role of dielectric quenching and capillary condensation effects, Phys. stat. Sol. (c) 2(2005) 3481-3485.

致 謝

離開自己的家鄉和祖國，冒險去一個我并不會講當地語言的國外大學攻讀博士學位，是我一生做出的最艱難的決定。很榮幸能夠在朝鮮大學光學納米材料實驗室從事研究工作。三年來，我成果的取得是研究組團體直接或間接積纍與貢獻的結果。轉眼間，讀博生涯即將結束，回首過去的點點滴滴，仍記憶猶新，自己有著很多的收穫和感悟，也經歷了許多喜悅、痛苦、挫折、成功……。這些都是我人生重要的一筆財富。

我要衷心的感謝博士生導師孫洪來教授。幾年來，孫教授給與了我持續的指導，熱情的幫助和全力的支持。能有這樣非凡的人指導我的博士研究工作讓我榮幸之至，在此向他崇高的敬意！！

由於語言障礙，我在韓國學習和生活并不自如。感謝實驗室往届和在读成员的直接幫助和支持，特別是Kyungkuk Koh博士、Jongjun Kim博士、Daeyoon Jung博士、Bomina Shin博士、孟加拉国的Banna博士以及以及Jinkyue Ree博士。向Kim Ho-Joong教授及其實驗室成員，表示真摯的感謝。

我還要感謝我的朋友們，特別是已入读高丽大学的邵疆疆—我最親密的學弟；以及共同生活在綠色家園，曾經互相關心互助的朋友們。此外，來自越南的Nguyen Chi Tai和Nguyen Kha博士；印度的Seke博士，菲律賓的Taimi博士和Isabel博士、巴基斯坦的Adnan和Zahid博士、非洲肯尼亚的Antony博士、馬來西亞的Bihlii博士，還有蒙古國的Puujee和Zolboo兩位醫學朋友。十分榮幸和你們成爲朋友，你們的陪伴讓我在韓國充滿了歡樂。

我會永遠懷念朝鮮大学櫻花漫天飛舞的校園，以及光州清幽美麗的無等山。

衷心感謝滄州師範學院云電軍書記！來韓前我曾惴惴不安，云書記多次給予鼓勵，他堅定有力的神情，語重心長的話語仿佛就在昨日。感謝學校和各位領導對我的厚愛和支持，讓我獲得了外出學習深造的機會。期待回國後為學校，為滄州的教育事業和科技發展做出微薄的貢獻。祝福我們的學校蒸

蒸日上，越來越好！祝福學校的老師和同學們！！

特別感謝我的師父-滄州師範學院副校長範小振先生。先生是我教學和科研起步的引路人，又是我攻讀博士學位的鑒定支持者。正有了您的循循善誘、啓發、鼓勵、幫助和關懷，我才以足夠的毅力和信念完成博士學業。先生嚴謹的治學態度、堅持不懈的科學精神、樸實謙遜的處事風格和積極向上的人生態度將激勵和影響我的一生。

誠摯地感謝化學與化工學院領導和同事們对我的關懷，鼓勵以及日常的幫助；還有國際交流學院、人事處、財務處等部門的助力。不能忘記齊越傳媒學院的閆軍博士，計算機科學與工程學院的劉霞老師，美術學院的王雪博士，在繪圖方面爲我提供了很大的幫助。感謝滄州師範學院和我保持密切聯係的朋友們，你們的聯係和幫助很重要，陪我度過了孤獨和艱難的日子。

謹以此論文獻給我最愛的家人。我的妻子王占麗對我無條件的支持和理解，父母對家庭的全力投入，給予了我無窮的力量。可我並沒有給予他們足夠的愛和關心。我的兒子周家好，從一歲起就缺少父親的陪伴，所幸適應和成長的很好。姑姑和妹妹一直在關心鼓勵著我。冥冥之中祖父也在保佑著我，助我成功化解每一次科研中的困境。值此之際，僅向所有支持、幫助、關懷和鼓勵我的親人和朋友表示真摯的感謝！！

感謝祖國多年來的培養！個人的命運與祖國的未來息息相關。“此生無悔入華夏，來生愿在種花家”！！祝福偉大的祖國繁榮富强，早日實現中華民族的偉大復興的中國夢！！！

周自成　于韓國光州

2020.05.18

ACKNOWLEDGEMENTS

The decision to leave my family and venture into a country where I could not speak their language was one of the biggest and hardest decisions I have ever made. I am feeling grateful to be able to work in photonic nanomaterials laboratory and complete this Doctoral research project. The success of this project is the outcome of accumulated contributions from numerous great individuals and organizations, either directly or indirectly. In an instant, the career of doctorate life is coming to an end, Looking back every bit of the past, I still have a fresh momory and too much sense and gains, and also experienced a lot of joy, pain, frustration, success……These are all important treasures in my life.

Foremost, I would like to express my sincere gratitude and appreciations to my research advisor, Professor Sohn Hong-lae for his continual guidance, enthusiasm and support that he has provided me throughout the years. I could not be more fortunate to have such extraordinary person who guides me through this work. Pay high tribute to him here!!

My stay in Korea may not be as smooth as it would be due to my language barrier. I would like to thank the former and current members of the Photonic Nanomaterials Laboratory for their direct support and assistances, particularly to Dr. Kyungkuk Koh, Jongjun Kim, Daeyoon Jung, Bomina Shin, Banna and Jinkyue Ree. Besides, I have to acknowledge Professor Kim Ho-Joong and his lab members for the assistance they have

given to me.

I would like to express my heartfelt gratitude to my great buddies, particularly to Shao Jiang-jiang, my close younger brother who is studying in Korea University, and my dear friends who lived in Green village which always helped and concorned each other. Besides, my international friends, especially, Dr.Nguyen Chi Tai and Nguyen Kh in biochemistry who come from Vietnam, Seke from Inida, Taimi and Isabel from Philippines, Adnan and Zahid from Pakistan, Antony from Kenya, Africa, Bihlii from Malaysia, and two medical friends of Puujee and Zolboo from Mongolia. I am very honoured to be friends with all of you. Your accompany brighten up my stay in Chosun University.

I will always miss the flying cherry blossoms of campus of Chosun University and the secluded and beautiful Mudeung Mountain.

I could not thank you enough to Secretary Yun Dian-jun of the Party Committee of Cangzhou Normal University. I worried too much about made decision of go abroad. Secretary Yun encouraged me again and again. His steadfastandpotentspirit,the sincerity and affection words,seemed like only yesterday.Thanks for the great kindness and support of our University and the leaders ,then I got the opportunity of go abroad for further studying. I am looking forward to make modest contribution to the education process and development of science and technology for our university and Cangzhou region. Best wishes for better and better to our university. Send my regards to teachers and students!!

I would like to express my heartfelt appreciation to the Vice President of Cangzhou Normal University, Professor Xiao-zhen Fan, who is the supervisor for my teaching, scientific research, and also the unwavering supporter of my ph.D. studying. With professor's systematic guidance, enlightenment, encouragement, favour and solicitude, and then I achieved my doctorate with continuous perseverance and faith. Professor Fan's rigorous attitude of scholarship, unremitting scientific spirit, plainness and modesty style of life, and the positive attitude toward life are inspiring and guiding all my life.

For their care, hearten and daily help, thanks to the leaders and colleagures of school of Chemistry and Chemical Engineering, as well as the assistance of International Exchange College, Departments of Personnel and Finance. It should be also mentioned that Dr. Yan Jun from College of Communication Qi Yue, Mrs Liu Xia from College of Computer Science and Engineering, Dr. Wang Xue from of fine arts,who provided me a lot of assistance in drawing. Not forgotten are the groups of close friends and colleagues, also include the for me and current students who stay in touch with me from Cangzhou Normal University. Your presences and helps do mean a lot to me to get through loneliness and hard time in Korea.

I would like to respectfully present this thesis and my very special thank goes to my dearest family. My wife, WangZhan-Li for her unconditional love and understanding, and my parents devoted all their time and energy into dedication to my family for the last several years,which gave me endless strength. However,I have failed to care enough. My thanks to you

are boundless. My son -Zhou Jia-Hao, who grow up and adapt well without y resence ince year old. My aunt and younger sister,who always there to support me. In the unseen world, my grandfather always blessed me successfully resolve the difficulties of every scientific research.

Thanks for the cultivation of motherland for decades. Personal destiny is closely related to the future of the motherland. “No regrets to enter China in this life, I would like to cultivating flowers for my motherland in the next life”. Wish the prosperous of our great motherland, and realize the Chinese dream of the great national renewal at an early date!!!

Zicheng Zhou,
In Gwangju, Korea
18th May, 2020